

# Topological Quenching of Spin Tunneling in $\text{Mn}_{12}$ -acetate Molecules

Chang-Soo Park\* and Anupam Garg

*Department of Physics and Astronomy, Northwestern University, Evanston, Illinois 60208*

(November 20, 2018)

## Abstract

We investigate the topological quenching of spin tunneling in  $\text{Mn}_{12}$ -acetate molecules with an applied magnetic field along the hard axis. The model Hamiltonian describing this system has a fourth-order term due to the tetragonal anisotropy. We treat this model using the discrete phase integral formalism in which the Schrödinger equation corresponding to the Hamiltonian becomes a nine-term recursion relation. We solve this recursion relation and find that the tunnel splitting is quenched at certain values of the applied field. We also present a qualitative treatment based on the instanton approach.

75.10Dg, 03.65.Db, 03.65.Sq, 75.45.+j, 75.50.Xx

## I. INTRODUCTION

Quantum tunneling of a spin or spin-like degree of freedom has been discussed for over a decade now [1], but unambiguous evidence for its existence has only come recently [2] from studies on the magnetic molecule  $[\text{Fe}_8\text{O}_2(\text{OH})_{12}(\text{tacn})_6]^{8+}$  ( $\text{Fe}_8$  for short). This molecule has a total spin  $S = 10$ , is biaxially symmetric, and can be modeled by the spin Hamiltonian

$$\mathcal{H} = k_1 S_x^2 + k_2 S_y^2 - g\mu_B \mathbf{S} \cdot \mathbf{H}, \quad (1.1)$$

with  $k_1 > k_2 > 0$ . In the first approximation, it has two degenerate ground states, approximately given by  $S_z = \pm 10$ , which are separated by an energy barrier in the  $xy$ -plane. The question of interest is to understand how these states are admixed by quantum tunneling.

Direct numerical diagonalization of Eq. (1.1) using the experimentally determined values  $k_1 \simeq 0.33$  K,  $k_2 \simeq 0.22$  K [3–5] reveals that the tunnel splitting  $\Delta$  is  $\sim 10^{-9}$  K, which is too small to be observed directly. Wernsdorfer and Sessoli [2] overcome this difficulty by applying a small amplitude ac magnetic field along the  $z$  direction, which causes the  $S_z = \pm 10$  levels to cross one another. Transitions between these levels are now possible via the Landau-Zener-Stückelberg (LZS) process [6], and the underlying tunneling matrix element  $\Delta$  can be deduced from a measurement of the incoherent LZS relaxation rate for the total magnetization. The key experimental fact that supports this interpretation of the relaxation (which could after all be due to a classical activation process a priori), is a systematic and remarkable oscillatory dependence of the inferred splitting  $\Delta$  on the strength of the magnetic field  $\mathbf{H}$  when this field is applied along the hard direction  $\hat{\mathbf{x}}$ . This phenomenon was predicted some time ago [7] based on an instanton approach. Briefly, when  $\mathbf{H} \parallel \hat{\mathbf{x}}$ , there are two symmetry related instanton paths that wind around  $\hat{\mathbf{x}}$  in opposite directions, and together form a closed loop on the (complexified) unit sphere. The actions for the instantons are complex, and differ by a real valued Berry phase given by  $S$  times the area of the loop, giving rise to interference [8]. Now, however, the Berry phase is not fixed at  $2\pi S$ , but may be continuously varied by varying  $H$ . As a function of  $H$ , therefore, the tunnel splitting oscillates, and is completely quenched at values of  $H$  where the Berry phase is an odd integer times  $\pi$ .

In this paper, we wish to study topological quenching of tunneling in a second magnetic molecule,  $\text{Mn}_{12}$ -acetate (or  $\text{Mn}_{12}$ -ac for short), which has also been the subject of several experimental studies [9–13]. The reason for our interest in  $\text{Mn}_{12}$ -ac is that, in contrast to  $\text{Fe}_8$ , it has tetragonal symmetry. The spin Hamiltonian of  $\text{Mn}_{12}$ -ac can be written as

$$\mathcal{H} = -AS_z^2 - BS_z^4 + C(S_+^4 + S_-^4), \quad (1.2)$$

where  $A \gg B \gg C > 0$ . The easy axis  $z$  now has four fold symmetry, the hard axes are  $\pm x$  and  $\pm y$ , and the medium axes are the lines  $y = \pm x$  in the  $xy$ -plane. Here, the symmetry of a pair of instanton paths is preserved when a magnetic field is applied along one of the four hard axes. Thus, the quenched spin tunneling phenomenon is also anticipated in  $\text{Mn}_{12}$ -ac. Whether it can be observed or not depends on how strong the environmental decoherence is, and is a question that we shall not investigate here.

To investigate the topological quenching of the spin tunneling in  $\text{Mn}_{12}$ -ac molecules we use the discrete phase integral (DPI) (or, discrete WKB) method [14,15]. The DPI method

has been applied to spin tunneling problems in a recent series of works by one of us (AG) [16–19]. This method is semiclassical just as the instanton approach is, but it is easier to use for the study of the splittings of higher pairs of levels. It is particularly well suited to study tunneling when  $\mathbf{H}$  is not along the hard axis. As in  $\text{Fe}_8$ , we anticipate that  $\Delta$  will be quenched at a number of such field values [17,20], which correspond to non-trivial diabolical points [21,22] in the magnetic field space. In this paper, however, we shall not consider such general orientations of the field as the calculations for  $\mathbf{H} \parallel \hat{\mathbf{x}}$  are already quite complex.

In the following section we present the DPI formalism for the present model. Unlike the previously studied model for  $\text{Fe}_8$ , the Schrödinger equation corresponding to the spin Hamiltonian for  $\text{Mn}_{12}\text{-ac}$  becomes a nine-term recursion relation because of the fourth-order term. We give a systematic analysis for this recursion relation. We then calculate the tunnel splittings as a function of the applied field for the first few energy levels. The results will be compared with those obtained by numerical diagonalization of the spin Hamiltonian. In Sec. III we give a qualitative discussion of spin tunneling based on the instanton approach. This gives a good physical picture of the quenched spin tunneling and explains some of the interesting features found in the DPI results. A summary of the results in Sec. IV concludes the paper.

## II. DPI CALCULATION OF TUNNEL SPLITTINGS

We consider the spin Hamiltonian in Eq. (1.2) with magnetic field applied along the  $x$  axis. For convenience we divide the Hamiltonian by  $A$  to work with dimensionless quantities. With this choice we can write

$$\mathcal{H} = -S_z^2 - \lambda_1 S_z^4 + \lambda_2 [S_+^4 + S_-^4] - \bar{S} h_x S_x, \quad (2.1)$$

where  $\lambda_1 = B/A$ ,  $\lambda_2 = C/A$ ,  $h_x = H_x/\bar{S}H_c$  ( $H_c \equiv A/g\mu_B$ ), and

$$\bar{S} = S + \frac{1}{2}. \quad (2.2)$$

Here,  $\mu_B$  is the Bohr magneton,  $g = 2$ , and  $S$  is the spin. Following Ref. [13],  $A/k_B = 0.556\text{K}$ ,  $B/k_B = 1.1 \times 10^{-3}\text{K}$ ,  $C/k_B = 3 \times 10^{-5}\text{K}$ , so that  $\lambda_1 = 1.98 \times 10^{-3}$ ,  $\lambda_2 = 5.4 \times 10^{-5}$ , and  $H_c = 0.414\text{T}$ . Let  $|\hat{\mathbf{n}}\rangle = |\theta, \phi\rangle$  be the spin coherent state with maximal spin projection along the direction  $\hat{\mathbf{n}}$ , with spherical coordinates  $\theta$  and  $\phi$ . We introduce the classical energy

$$\begin{aligned} \mathcal{H}_c(\theta, \phi) &= \langle \hat{\mathbf{n}} | \mathcal{H} | \hat{\mathbf{n}} \rangle \\ &= -S^2 \cos^2 \theta - \lambda_1 S^4 \cos^4 \theta + 2\lambda_2 S^4 \sin^4 \theta \cos 4\phi - S\bar{S}h_x \sin \theta \cos \phi. \end{aligned} \quad (2.3)$$

When  $h_x = 0$ ,  $\mathcal{H}_c$  has minima at  $\theta = 0$ ,  $\theta = \pi$ . As  $h_x$  is increased, these minima move toward  $\theta = \pi/2$ ,  $\phi = 0$ , lying in the  $xz$ -plane. At a certain critical field,  $h_{xco}$ , these minima will merge with each other, giving rise to a double zero of  $\partial\mathcal{H}_c(\theta, \phi = 0)/\partial\theta$  at  $\theta = \pi/2$ . By using this condition, we can show that

$$h_{xco} = \frac{2S}{\bar{S}} (1 + 4\lambda_2 S^2). \quad (2.4)$$

With the experimental numbers given above,  $h_{xco} = 1.946$  [23].

## A. Recursion Relation

The DPI formalism can be started with Schrödinger equation in the  $S_z$  representation. Introducing  $\mathcal{H}|\psi\rangle = E|\psi\rangle$ ,  $S_z|m\rangle = m|m\rangle$ ,  $\langle m|\psi\rangle = C_m$ , and  $\langle m|\mathcal{H}|m'\rangle = t_{m,m'}$ , the Schrödinger equation corresponding to the Hamiltonian (2.1) can be expressed as

$$\sum_{n=m-4}^{m+4} t_{m,n} C_n = E C_m. \quad (2.5)$$

This is a nine-term recursion relation with diagonal terms  $t_{m,m}$  from  $S_z^2$  and  $S_z^4$ , and off-diagonal terms  $t_{m,m\pm 1}$ ,  $t_{m,m\pm 4}$  which are from the  $S_x$  and  $S_\pm^4$  parts, respectively. Since there are no  $S_\pm^2$  or  $S_\pm^3$  terms in the Hamiltonian, we have  $t_{m,m\pm 2} = t_{m,m\pm 3} = 0$ .

The recursion relation (2.5) may be interpreted as the Schrödinger equation of an electron in a one-dimensional tight binding model. That is, we can consider the diagonal and off-diagonal terms as the on-site energy and hopping terms, respectively. Once this analogy is recognized, assuming  $t_{m,m\pm\alpha}$  ( $\alpha = 0, 1$ , or  $4$ ) vary slowly with  $m$ , we can treat the recursion relation within a continuum quasiclassical approximation or a phase integral method [18,14,15]. With this approximation we can define smooth functions

$$t_\alpha(m) \simeq \frac{1}{2}(t_{m,m+\alpha} + t_{m,m-\alpha}), \quad \alpha = 0, 1, 4. \quad (2.6)$$

For the present model,  $t_\alpha$ 's are given by

$$\begin{aligned} t_0(m) &= -m^2(1 + \lambda_1 m^2), \\ t_1(m) &= -\frac{\bar{S}h_x}{2}\sqrt{\bar{S}^2 - m^2}, \\ t_4(m) &= \lambda_2(\bar{S}^2 - m^2)^2, \end{aligned} \quad (2.7)$$

where we have used the approximation  $S(S+1) \approx \bar{S}^2$ . Introducing the DPI wavefunction within the semiclassical approximation

$$C_m \sim \frac{1}{\sqrt{v(m)}} \exp \left[ i \int^m q(m') dm' \right], \quad (2.8)$$

we have the Hamilton -Jacobi equation

$$E = \mathcal{H}_{sc}(q, m) \equiv t_0(m) + 2t_1(m) \cos q + 2t_4(m) \cos 4q, \quad (2.9)$$

and the transport equation

$$\begin{aligned} v(m) &= \frac{\partial \mathcal{H}_{sc}}{\partial q} \\ &= -2 \sin q(m) [t_1(m) + 16t_4(m) \cos q(m) \cos 2q(m)]. \end{aligned} \quad (2.10)$$

In Eqs. (2.8) and (2.10),  $q(m)$  is a local,  $m$ -dependent Bloch wave vector obtained by solving Eq. (2.9) for  $q$  for any given energy  $E$ . It is very useful to have a physical picture of these equations. For a given value of  $m$ , Eq. (2.9) gives an energy band  $E(q)$  which defines the

classically allowed range of energies. In Fig. 1 we show possible  $E$  vs.  $q$  curves for our problem. At lower and upper edges of the band the transport equation shows that  $v(m)$  becomes zero because the slope  $\partial E(q)/\partial q$  is zero. This means the band edges are related to the classical turning points. These are not the only turning points, however. Such points are more generally defined by the condition that the velocity  $v(m)$  vanishes. This condition produces additional loci in  $E - m$  space, which we call *critical curves*, along with the  $m$ -dependent band edges. These curves are crucial to understanding how the oscillating tunnel splitting, i.e., the quenching effect, appears.

## B. Critical Curves

From Eq. (2.10) the condition  $v(m) = 0$  is satisfied when  $q = 0$ , or  $q = \pi$ , or  $q = q_*$ , where  $q_*$  is the solution of

$$32 t_4(m) \cos^3 q_*(m) - 16 t_4(m) \cos q_*(m) + t_1(m) = 0. \quad (2.11)$$

Substituting these into Eq. (2.9) we obtain the following energy curves for each of the three  $q$ 's

$$\begin{aligned} U_0(m) &= t_0(m) + 2t_1(m) + 2t_4(m), \\ U_\pi(m) &= t_0(m) - 2t_1(m) + 2t_4(m), \\ U_*(m) &= t_0(m) + 2t_1(m) \cos q_*(m) + 2t_4(m) \cos 4q_*(m), \end{aligned} \quad (2.12)$$

where  $U_0(m) \equiv E(0, m)$ ,  $U_\pi(m) \equiv E(\pi, m)$ , and  $U_*(m) \equiv E(q_*(m), m)$ . Whenever a given energy  $E$  crosses one of these curves a turning point occurs. Various types of turning points depending on the characteristic of the critical curves have been analyzed in Ref. [18]. An interesting feature of this analysis is the existence of novel turning points inside the classically forbidden region, which is crucial for the quenching of spin tunneling. The recursion relation studied there was based on a spin Hamiltonian which includes terms up to second order, and there were only three critical curves to be considered. Here, we expect to have up to five curves,  $U_0(m)$ ,  $U_\pi(m)$ , and up to three  $U_*(m)$ 's from the cubic equation (2.11).

In order to proceed further, it is necessary to analyze the critical curve structure more closely, in particular, its dependence on  $h_x$ . To do this, let us first compare  $U_0(m)$  with  $U_\pi(m)$ . From Eq. (2.7) it can be easily seen that  $U_\pi(m) > U_0(m)$  since  $t_0(m) < 0$ ,  $t_1(m) < 0$ , and  $t_4(m) > 0$  for all  $|m| < \bar{S}$ . Thus,  $U_\pi(m)$  can be the upper band edge. However, in order for this to be so we still need to prove that  $U_\pi(m) > U_*(m)$ . This is not obvious. Indeed, since the Eq. (2.11) is a cubic in  $\cos q_*$ , it is possible to have complex solutions. These solutions will yield a complex  $U_*(m)$ , which is not of interest because the Hamilton-Jacobi equation  $E = U_*(m)$  can not then be satisfied. A careful consideration of the solutions of Eq. (2.11) is therefore necessary.

Defining  $x = \cos q_*$ ,  $\mu = m/\bar{S}$ , and using Eq. (2.7) for the  $t_\alpha$ 's, we can write Eq. (2.11) as

$$f(x) \equiv 2x^3 - x - \frac{h_x}{32\lambda_2\bar{S}^2}(1 - \mu^2)^{-3/2} = 0. \quad (2.13)$$

A sketch of the function  $f(x)$  is drawn in Fig. 2. This sketch incorporates the following easily verified properties of  $f(x)$ : (i)  $f(0) < 0$ , (ii)  $f'(0) = -1$ , (iii)  $f'(\pm 1) = 5 > 0$ , (iv)  $f(-1) < 0$ , (v)  $f(1)$  may be of either sign, (vi)  $f'(\pm 1/\sqrt{6}) = 0$ , where  $f'(x) \equiv df(x)/dx$ . It follows that a curve of type marked (a), characterized by one real zero of  $f(x)$  arises when  $h_x$  is large, or when  $|m|$  is large, and that a curve of type marked (b), characterized by three real zeros arises when  $h_x$  is small, or when  $|m|$  is small. Let us denote the largest zero by  $x_1$ , and the other two, when they are real, by  $x_2$  and  $x_3$  with  $x_2 > x_3$ . The corresponding values for  $q_*(m)$  and  $U_*(m)$  are denoted by  $q_{*i}$  and  $U_{*i}(m)$ , with  $i = 1, 2$ , or  $3$ . It is obvious that  $x_1 > 0$ , and that  $-1 < x_3 < -\frac{1}{\sqrt{6}} < x_2 < 0$ . The first real root yields a positive value for  $\cos q_{*1}$ , but since we cannot say if  $x_1$  is greater or lesser than 1,  $q_{*1}$  may be real or pure imaginary. The other two real roots, when they exist, always yield real wavevectors  $q_{*2}$  and  $q_{*3}$ .

The transition from one to three real roots occurs when  $f(x)$  has a double zero, i.e.,  $f(x)$  and  $f'(x)$  both vanish simultaneously. It is easily shown that this condition is equivalent to

$$h_{xc}(m) = h_{x\max} \left( 1 - \frac{m^2}{\bar{S}^2} \right)^{3/2}, \quad (2.14)$$

$$h_{x\max} = 32 \sqrt{\frac{2}{27}} \lambda_2 \bar{S}^2. \quad (2.15)$$

The curve  $h_{xc}(m)$  and some special values of  $h_x$  are displayed in Fig. 3. The physical meanings of these values are listed in Table I. From the arguments of the previous paragraph, it follows that we will have three zeros when  $h_x < h_{xc}(m)$ , and one zero when  $h_x > h_{xc}(m)$ . When  $h_x < h_{x\max}$ , we can also ask for the points  $\pm m_a(h_x)$  at which we change from one to three real roots of  $f(x)$ . These are directly given by solving Eq. (2.14) for  $h_{xc}(m) = h_x$ :

$$m_a = \bar{S} \left[ 1 - \left( \frac{h_x}{h_{x\max}} \right)^{2/3} \right]^{1/2}. \quad (2.16)$$

Next, let us investigate whether  $U_{*1}(m)$  is inside or outside the classically allowed energy band. Since  $x_1$  moves to larger positive values as  $|m|$  increases (see Fig. 2), we see that  $U_{*1}$  lies inside the band if  $x_1 < 1$ , i.e.,  $|m| < m_*$ , where  $m_*$  is such that  $f(1) = 0$ . Solving this equation we get

$$m_* = \bar{S} \left[ 1 - \left( \frac{h_x}{h_{xr}} \right)^{2/3} \right]^{1/2}, \quad (2.17)$$

$$h_{xr} = \sqrt{\frac{27}{2}} h_{x\max}. \quad (2.18)$$

Clearly,  $m_a < m_*$ .

Let us also explore whether the  $U_{*i}(m)$ 's, when they are real, are larger or smaller than  $U_\pi(m)$  or  $U_0(m)$ . We consider the following differences:

$$\begin{aligned} U_{\pi j}(m) &\equiv U_\pi(m) - U_{*j}(m) \\ &= 16t_4(m) \cos q_{*j} (1 + \cos q_{*j})^2 (-2 + 3 \cos q_{*j}), \end{aligned} \quad (2.19)$$

$$\begin{aligned}
U_{*ij}(m) &\equiv U_{*i}(m) - U_{*j}(m) \\
&= -16t_4(m)(\cos^2 q_{*i} - \cos^2 q_{*j}) \left[ 3(\cos^2 q_{*1} + \cos^2 q_{*j}) - 1 \right], \tag{2.20}
\end{aligned}$$

$$\begin{aligned}
U_{0i}(m) &\equiv U_0(m) - U_{*i}(m) \\
&= 16t_4(m) \cos q_{*i} (1 - \cos q_{*i})^2 (2 + 3 \cos q_{*i}), \tag{2.21}
\end{aligned}$$

where  $i, j = 1, 2$ , or  $3$  and we have used Eq. (2.11) to eliminate  $t_1(m)$  in favor of  $t_4(m)$ . From these equations, and using the facts that  $t_4(m) > 0$ , plus [24]

$$-\frac{1}{\sqrt{2}} \leq \cos q_{*3} \leq -\frac{1}{\sqrt{6}} \leq \cos q_{*2} < 0, \quad \frac{1}{\sqrt{2}} \leq \cos q_{*1}, \tag{2.22}$$

we find :

1. When there is only one real root,

$$U_{*1}(m) < U_0(m) < U_\pi(m) \tag{2.23}$$

for all  $|m| < \bar{S}$  and  $h_{x\max} < h_x < h_{xco}$ .

2. When there are three real roots,

$$U_{*1}(m) < U_0(m) < U_{*3}(m) < U_{*2}(m) < U_\pi(m) \tag{2.24}$$

for  $h_{xi} < h_x$ ,

$$U_{*1}(m) < U_{*3}(m) < U_0(m) < U_{*2}(m) < U_\pi(m) \tag{2.25}$$

for  $0 < h_x < h_{xi}$ , where  $h_{xi}$  is determined by  $U_0(m=0, h_{xi}) = U_{*3}(m=0, h_{xi})$ , which from Eqs.(2.21) and (2.22), is equivalent to  $\cos q_{*3}(m=0, h_{xi}) = -2/3$ .

We can now list the various types of critical curve patterns that arise in our problem, and the corresponding ranges of the field  $h_x$ . In the following,  $U_-(m)$  and  $U_+(m)$  denote the lower and upper bounds of the energy band, and  $U_f(m)$  and  $U_i(m)$  mean the forbidden and internal energies, respectively.

Case I :  $h_{xr} < h_x < h_{xco}$ .

In this case  $U_{*2}$  and  $U_{*3}$  are not real for any  $m$ , and  $q_{*1}(m)$  is imaginary, i.e.,  $U_{*1}(m)$  is outside the band for all  $|m| \leq \bar{S}$ . The energy band  $E(q)$  is of the type in Fig. 1a for all  $m$ , and the critical curves become

$$U_{*1} = U_f, \quad U_0 = U_-, \quad U_\pi = U_+ \quad \text{for } |m| < \bar{S}, \tag{2.26}$$

which are shown in Fig. 4.

Case II :  $h_{x\max} < h_x < h_{xr}$ .

Now,  $U_{*2}$  and  $U_{*3}$  continue to be complex for all  $m$ , but  $q_{*1}(m)$  is real in the central region  $|m| < m_*$ . In this region, the energy band is as in Fig. 1b, while in the outer region it is of the type in Fig. 1a. Accordingly, the critical curves have the structure shown in Fig. 5 and can be written as

$$\begin{aligned}
U_{*1} &= U_-, \quad U_0 = U_i, \quad U_\pi = U_+ && \text{for } |m| < m_*, \\
U_{*1} &= U_f, \quad U_0 = U_-, \quad U_\pi = U_+ && \text{for } |m| > m_*.
\end{aligned} \tag{2.27}$$

Case III :  $0 < h_x \leq h_{x\max}$ .

There are now three  $m$  regions. In the outer region,  $|m| > m_*$ ,  $U_{*2}$  and  $U_{*3}$  are still complex,  $U_{*1}$  is outside the band, and  $E(q)$  has the shape in Fig. 1a. In the intermediate range  $m_a < |m| < m_*$ ,  $U_{*2}$  and  $U_{*3}$  continue to be complex, but  $U_{*1}$  is inside the band, and  $E(q)$  has the shape in Fig. 1b. In the central range,  $|m| < m_a$ ,  $U_{*2}$  and  $U_{*3}$  become real, and  $E(q)$  has the shape shown in Figs. 1(c) (when  $h_{xi} < h_x < h_{x\max}$ ) and (d) (when  $h_x < h_{xi}$ ). The critical curves can be expressed as [25]

$$\begin{aligned} U_0, U_{*2}, U_{*3} = U_i, U_{*1} = U_-, U_\pi = U_+ & \quad \text{for } |m| < m_a, \\ U_0 = U_i, U_{*1} = U_-, U_\pi = U_+ & \quad \text{for } m_a < |m| < m_*, \end{aligned} \quad (2.28)$$

which are illustrated in Figs. 6a and 6b.

As a matter of fact, we should distinguish two subcases in Case III. When  $h_x > h_{xi}$ , as in Eq. (2.24), the relevant critical curves are as in Fig. 6a. When  $h_x < h_{xi}$ , as in Eq. (2.25), there is a range of  $m$  values in which  $U_{*3} < U_0$  (see Fig. 6b). For the experimental parameters relevant to Mn<sub>12</sub>-ac, the field  $h_{xi}$  is rather small, and the points  $m_0$ ,  $m_*$ ,  $m_a$ , and  $m_i$  are all clustered tightly near  $m = \bar{S}$ . This means that for the low lying states, there will be four turning points very close to one another, and the DPI analysis would have to be done using a *quartic* turning point formula, analogous to the quadratic turning point formula as discussed by Berry and Mount [26]. Since we know the qualitative structure of the energy spectrum for fields as small as  $h_{xi}$ , based on the arguments of Sec. III, e.g., this exercise is largely academic, and we have chosen not to perform it. This means that our analysis is not quite correct at very small fields, and this can be seen in Fig. 7 especially in the behavior of the splitting between the first excited pair of levels. As we shall discuss in Sec. III, this splitting is rigorously zero at  $h_x = 0$ , whereas we appear to find a zero at a slightly non-zero value of  $h_x$ .

As discussed in Ref. [19] the quenching of spin tunneling occurs when  $q(m)$  has a real part as well as an imaginary part inside the forbidden region. From the viewpoint of energy curves this happens when there is an energy curve inside the forbidden region. From the above analysis we can see that only  $U_{*1}(m)$  resides inside the forbidden region. For a given energy  $E$  such that  $U_{0\min} \leq E < U_{*1\max}$ ,  $q$  changes from pure imaginary to complex as  $m$  passes from the  $|m| > m_c$  region to the  $|m| < m_c$  region, where  $m_c$  is the point where  $E$  intersects  $U_{*1}(m)$ , (for example see Fig. 4). When  $q$  becomes complex the semiclassical wavefunction in Eq. (2.8) oscillates with exponentially decaying or growing envelope. The quenching of spin tunneling arises from this oscillating nature of the wavefunction inside the forbidden region.

We note here that for the experimental Mn<sub>12</sub> parameters, the field  $h_{x\max}$  is quite small (see the legend in Fig. 3), and so in the entire field range for Case III, even though there is a forbidden region turning point, the behavior of the ground state tunnel splitting is qualitatively similar to that for  $h_x = 0$ . The behavior of the splitting of the next two levels is more interesting, and as can be seen from Fig. 7, the DPI method does capture it, at least qualitatively, and perhaps even quantitatively.

### C. Tunnel Splittings

We now calculate the energy splitting due to the spin tunneling between degenerate states in Mn<sub>12</sub>-acetate. In Ref. [19], tunnel splittings for five-term recursion relation have been obtained from Herring's formula. The final result is, however, quite general so that it can be applied to a recursion relation which includes more than five terms. Moreover, as we can notice from the above classifications, although the present nine-term case has more critical curves the possible types of the turning points are all included in those discussed in Ref. [18], and no new type of turning point emerges here. Thus, we can directly apply the formula for the tunnel splittings obtained in Ref. [19] to the present problem. Since our calculation is based on this formula we quote the main results here. The tunnel splitting for  $n$ th pair of states is given by

$$\Delta_n(h_x) = \frac{1}{n!} \sqrt{\frac{8}{\pi}} \omega_0 F^{n+\frac{1}{2}} e^{-\Gamma_0} \cos \Lambda_n, \quad (2.29)$$

where

$$\begin{aligned} \Gamma_0 &= \int_{-m_0}^{m_0} \kappa_0(m) dm, \\ \Lambda_n &= \int_{-m_c}^{m_c} \left( \chi_0 + \left(n + \frac{1}{2}\right) \omega_0 \chi'_0 \right) dm, \\ F &= 2M\omega_0 (m_0 - m_c)^2 \\ &\quad \times \exp \left( -2Q_1 + \omega_0 \int_{-m_c}^{m_c} \kappa'_0 dm \right), \\ Q_1 &= \int_{-m_0}^{-m_c} \left( \frac{\omega_0 B'_0}{\sqrt{B_0^2 - 1}} + \frac{1}{m + m_0} \right) dm. \end{aligned} \quad (2.30)$$

Here,  $\kappa$  and  $\chi$  are the imaginary and real parts of complex  $q$ , respectively, and

$$\begin{aligned} \kappa_0 &= \kappa(m, \epsilon = 0); \quad \kappa'_0 = \left. \frac{\partial \kappa(m, \epsilon)}{\partial \epsilon} \right|_{\epsilon=0}, \\ \chi_0 &= \chi(m, \epsilon = 0); \quad \chi'_0 = \left. \frac{\partial \chi(m, \epsilon)}{\partial \epsilon} \right|_{\epsilon=0}, \\ B_0 &= \cos q(m, \epsilon = 0); \quad B'_0 = \left. \frac{\partial \cos q(m, \epsilon)}{\partial \epsilon} \right|_{\epsilon=0}, \end{aligned} \quad (2.31)$$

with  $\epsilon \equiv E - U_-(-m_0)$ . In these equations,  $\pm m_c$  are not quite the turning points of the previous subsection, in that they are not the point where  $U_{*1}(m)$  equals the true energy  $E_n$  of the  $n$ th pair of levels. Rather, they are the points where  $U_{*1}(m) = U_-(\pm m_0)$ , which corresponds to setting  $E = U_-(m_0)$ , i.e.,  $\epsilon = 0$ . The reason is that the formula (2.29) incorporates expansions of various phase integrals in the energy difference

$$\epsilon_n = E_n - U_-(m_0) = \left(n + \frac{1}{2}\right) \omega_0, \quad (2.32)$$

which is of order  $(1/S)$  compared to the energy barrier, as long as  $n \ll S$ . This is why  $m_c$  is modified, and also why the primary phase integral for the Gamow factor  $\Gamma_0$  runs from  $-m_0$

to  $m_0$ , the minima of  $U_0(m)$ , rather than between the points where  $U_0(m) = E_n$ . Since all energy curves are a function of both  $m$  and  $h_x$ , these points still depend on  $h_x$ , which in turn makes the  $\Delta_n$  depend on  $h_x$ .

The mass  $M$  and frequency  $\omega_0$  in Eq. (2.30) are obtained by approximating  $U_-(m)$  near its minima by a parabola, i.e.,  $U_-(m) = E + \frac{1}{2}m\omega_0^2(m \pm m_0)^2$ . For  $m = -m_0$  we find,

$$M = -\frac{1}{2t_1(-m_0) + 32t_4(-m_0)},$$

$$\omega_0^2 = -2[t_1(-m_0) + 16t_4(-m_0)] \left. \frac{\partial^2 U_-}{\partial m^2} \right|_{m=-m_0}. \quad (2.33)$$

The application of the formulas (2.29)-(2.33) cannot be carried out in closed form all the way, and we must resort to numerical methods. We explain the principal steps in our numerical calculation below.

In step 1, we must find  $\pm m_0$ , and  $U_-(\pm m_0)$ . For our problem we discover that  $U_-(m)$  is always given by  $U_0(m)$  near the classically allowed minima. The equation for the minima can be reduced to another cubic,

$$\bar{S}^2 h_x^2 = 4(\bar{S}^2 - y)[2(\lambda_1 - 2\lambda_2)y + 1 + 4\lambda_2 \bar{S}^2]^2, \quad (2.34)$$

where  $y = m^2$ . For the parameters  $\lambda_1$  and  $\lambda_2$  of interest to Mn<sub>12</sub>, and  $h_x < h_{xco}$ , all three roots of this cubic equation are real, but only one is positive. This root gives us  $m_0$ , and substitution of this value into Eq. (2.12) for  $U_0(m)$  gives  $E$ , and Eqs. (2.33) then give  $M$  and  $\omega_0$ .

Step 2 is to obtain the points  $\pm m_c$  given by the roots of the equation

$$U_{*1}(m) = U_-(m_0). \quad (2.35)$$

As discussed after Eq. (2.32), up to terms of relative order  $(1/S)$ , the points  $\pm m_c$  are the actual turning points for the low lying energies. Note that it is  $U_{*1}$  which appears in Eq. (2.35) since this is the critical curve that lies in the classically forbidden region.

To solve Eq. (2.35) numerically, we first solve Eq. (2.11) for the function  $\cos q_{*1}(m)$ , which can be done in closed form. This solution is then substituted in Eq. (2.12) to obtain  $U_{*1}(m)$ . The entire procedure can be implicitly implemented in the numerical routine. The same holds for  $dU_{*1}(m)/dm$ . Since  $U_-(m_0)$  is known from step 1, any of the standard root-finding methods—Newton-Raphson, bisection, secant etc.—can be applied to Eq. (2.35).

Step 3 is to find  $q(m)$ , in particular its real and imaginary parts  $\kappa_0(m)$  and  $\chi_0(m)$ . This is done by solving the Hamilton-Jacobi equation (2.9) with the energy  $E$  found in the first step. The problem amounts to solving a quartic equation in  $\cos q$  and making sure that one has the correct solution, which can be done easily by making use of the properties that we have found above. Thus in the region  $m_c < |m| < m_0$ , there are two solutions of the form  $i\kappa$  (with  $\kappa$  real), and two of the form  $\pi - i\kappa$ . We discard the latter, and of the former select that one which continuously tends to 0 as  $m \rightarrow \pm m_0$ . In the region  $|m| < m_c$ , the solutions can be written as  $i\kappa \pm \chi$ , and as  $\pi - (i\kappa \pm \chi)$ , where  $\chi \rightarrow 0$  as  $m \rightarrow \pm m_c$ . We discard the latter two, and read off  $\kappa(\equiv \kappa_0)$ , and  $\chi(\equiv \chi_0)$  from the imaginary and real parts of the first two. Note that both  $\kappa_0$  and  $\chi_0$  are taken to be positive.

Step 4 is to find the  $\epsilon$  partial derivatives  $\kappa'_0$  and  $\chi'_0$ , in effect  $\partial q(\epsilon, m)/\partial \epsilon$ . ( $B'_0$  is directly obtainable from  $\kappa'_0$ .) We differentiate the Hamilton-Jacobi equation with respect to  $E$ :

$$-2[t_1 \sin q + 4t_4 \sin 4q] \frac{\partial q}{\partial \epsilon} = 1. \quad (2.36)$$

Since  $q(m)$  is found in step 3, this equation gives  $\partial q/\partial \epsilon$  for any  $m$  directly.

We now have all the ingredients needed to evaluate the one-dimensional integrals  $\Gamma_0$ ,  $\Lambda_n$ ,  $F$ , and  $Q_1$ . This is a straightforward numerical procedure. The only point worth noting is that the integrand for  $Q_1$  is non-singular at  $m = -m_0$ , and behaves, in fact, as  $(m + m_0)$ .

In Fig. 7 we show the tunnel splittings for first three pairs of states as a function of the field parameter  $h_x$ . For comparison we also plotted the tunnel splittings obtained from exact diagonalization of the Hamiltonian.

From the results we observe several interesting features. First, as anticipated the tunnel splittings are completely suppressed at certain values of  $h_x$ . The overall pattern of zeros, their number, and the dependence of this number on  $n$ , the pair index, is understandable on general grounds as we shall discuss. What is surprising is how regularly spaced these values of  $h_x$  are. For the first pair of splittings, e.g., the intervals between successive zeros decrease by 2 or 3% only, and the last interval is 92% of the first. For the next pair,  $\Delta_2$ , the last interval is 95% of the first. The mean interval between zeros for the first three pairs is  $\Delta H_0 \simeq 0.93\text{T}$ ,  $\Delta H_1 \simeq 0.85\text{T}$ ,  $\Delta H_2 \simeq 0.79\text{T}$ .

The regularity of the zeros means that the phase integral  $\Lambda_n$  decreases almost linearly with  $h_x$ . (From Fig. 7, Gamow factor  $\Gamma_0$  also appears to be quite linear in  $h_x$ .) While this variation is clearly expected to be smooth, we have no a priori way to judge how linear it will be. A similarly strong regularity of quenching intervals is experimentally discussed in  $\text{Fe}_8$ . The simplest model Hamiltonian for  $\text{Fe}_8$  entails only second order terms in the components of the spin operator, and in this model, the spacing of zeros is exactly equal [28], but to describe actual  $\text{Fe}_8$ , one must add fourth-order terms. These terms change the spacing significantly, but still seem to preserve its regularity. It would be interesting to find a physical argument for this feature, which appears to be somewhat general.

Second, at  $h_x = 0$  the tunnel splitting alternates between zero and nonzero as the level number goes up. This is due to the fourth-order terms in the spin Hamiltonian. This term causes the tunneling in the  $\text{Mn}_{12}$  system, but it also restricts the transitions to the case that the difference,  $\Delta m = |m - m'|$ , between levels  $E_m$  and  $E_{m'}$  is a multiple of 4. For tunneling between degenerate states  $E_m$  and  $E_{-m}$  this requires the condition  $2m = 4p$ , where  $p$  is an integer. Therefore, there is no tunneling between  $+m$  and  $-m$  when  $m$  is an odd number.

To give a more detailed argument of this point, we note that when  $H_x = H_z = 0$ , because of the  $S_{\pm}^4$  terms, the Hamiltonian can be divided into the following subspaces for  $S = 10$ .

$$\begin{aligned} V_1 &= \{-10, -6, -2, +2, +6, +10\}, \\ V_2 &= \{-9, -5, -1, +3, +7\}, \\ V_3 &= \{-8, -4, 0, +4, +8\}, \\ V_4 &= \{-7, -3, +1, +5, +9\}, \end{aligned} \quad (2.37)$$

where the numbers in brackets give the  $m$  quantum numbers. The subspace  $V_1$  contains 6 levels, which form 3 pairs split by tunneling due to the  $CS_{\pm}^4$  terms. The space  $V_3$  contains

5 levels, of which  $\pm 8$ , and  $\pm 4$  are split by tunneling, and  $m = 0$  is isolated. There is no degeneracy amongst the 5 levels in space  $V_2$ , but because of time reversal, this space is isomorphic to  $V_4$ , and we therefore conclude that in the full spectrum of  $\mathcal{H}$ , there should be five pairs of *strictly* degenerate levels, corresponding approximately to  $m = \pm(2n + 1)$  with integer  $n$ .

Third, there are five quenching points in the ground and first excited states tunnelings, and the number of quenching points decreases as the level number goes up. For the ground state tunneling the allowed number of quenching points can be explained qualitatively by thinking in terms of instantons. Since the instanton approach also gives a good geometrical structure to the quenching we present it in a separate section.

### III. QUALITATIVE TREATMENT

In this section we give a qualitative treatment of the spin tunneling in  $\text{Mn}_{12}$  using instanton methods. Adding a hard axis field to Eq. (1.2), the Hamiltonian becomes

$$\mathcal{H} = -AS_z^2 - BS_z^4 + C(S_+^4 + S_-^4) - g\mu_B H_x S_x. \quad (3.1)$$

The instanton method is based on spin coherent state path integrals. In the spin coherent state representation the anisotropy energy corresponding to the Hamiltonian is given by

$$\begin{aligned} \mathcal{H}_c(\alpha, \beta) &= \langle \hat{\mathbf{n}} | \mathcal{H} | \hat{\mathbf{n}} \rangle \\ &= -AS^2 \sin^2 \alpha \sin^2 \beta - BS^4 \sin^4 \alpha \sin^4 \beta \\ &\quad + 2CS^4 (\cos^4 \alpha + \sin^4 \alpha \cos^4 \beta - 6 \sin^2 \alpha \cos^2 \alpha \cos^2 \beta) - g\mu_B H_x S \cos \alpha, \end{aligned} \quad (3.2)$$

where  $\alpha$  and  $\beta$  are the polar and azimuthal angles with respect to  $\hat{\mathbf{x}}$ , i.e.,

$$\begin{aligned} \cos \alpha &= \hat{\mathbf{n}} \cdot \hat{\mathbf{x}}, \\ \sin \alpha \cos \beta &= \hat{\mathbf{n}} \cdot \hat{\mathbf{y}} \\ \sin \alpha \sin \beta &= \hat{\mathbf{n}} \cdot \hat{\mathbf{z}}. \end{aligned} \quad (3.3)$$

The energy (3.2) exhibits two degenerate minima at  $\hat{\mathbf{n}}_i = (\alpha, \beta) = (\alpha_0, \pi/2)$  and  $\hat{\mathbf{n}}_f = (\alpha, \beta) = (\alpha_0, -\pi/2)$ , where  $\alpha_0 = \pi/2$  for  $H_x = 0$ , and decreases smoothly to 0 as  $H_x$  is increased. The level splitting due to tunneling between these minima can be obtained from the imaginary time propagator

$$\begin{aligned} K_{fi} &= \langle \hat{\mathbf{n}}_f | \exp[-\mathcal{H}T] | \hat{\mathbf{n}}_i \rangle \\ &= \int \mathcal{D}[\hat{\mathbf{n}}] \exp[-S_E[\hat{\mathbf{n}}(\tau)]], \end{aligned} \quad (3.4)$$

where

$$S_E[\hat{\mathbf{n}}(\tau)] = -iS\mathcal{A}[\hat{\mathbf{n}}(\tau)] + \int_0^T \mathcal{H}_c(\alpha, \beta) d\tau, \quad (3.5)$$

with

$$\mathcal{A}[\hat{\mathbf{n}}(\tau)] = \int_0^T (1 - \cos \alpha) \dot{\beta}(\tau) d\tau, \quad (3.6)$$

is the Euclidean action and complex in general. Here, the boundary conditions are  $\hat{\mathbf{n}}(0) = \hat{\mathbf{n}}_i$ ,  $\hat{\mathbf{n}}(T) = \hat{\mathbf{n}}_f$ . Geometrically, for a closed path, the integral in Eq. (3.6) can be interpreted as a surface area on the unit sphere enclosed by this path, which can be verified by Stokes theorem. In the large spin limit the path integral can be approximated by the sum of all contributions from paths that minimize the action, that is, the instanton paths. The instantons for the present model are not simple because of the fourth-order terms. However, we can construct a qualitative argument to find the quenching effect without performing explicit calculations. Since the Euclidean action  $S_E$  has both real and imaginary parts we can generally express the ground state tunnel splitting as

$$\Delta = \sum_j D_j e^{-S_{Rj}} e^{iS_{Ij}}, \quad (3.7)$$

where  $j$  labels the various instantons,  $S_{Rj}$ ,  $S_{Ij}$  are the real and imaginary parts of the instanton action, respectively, and  $D_j$  are prefactors. With these ingredients we now discuss how the quenching appears in the present model.

Let us first consider the case when  $H_x = 0$ . Since the energy has four-fold symmetry, an argument of von Delft and Henley can be applied [8]. If  $\hat{\mathbf{n}}(\tau)$  is an instanton path, so is  $\mathcal{R}_{\hat{\mathbf{z}}}(\pi/2)\hat{\mathbf{n}}(\tau)$ , where  $\mathcal{R}_{\hat{\mathbf{z}}}(\pi/2)$  is a rotation through  $\pi/2$  about  $\hat{\mathbf{z}}$ . Keeping in mind that  $\hat{\mathbf{n}}(\tau)$  is complex, when we project onto the real unit sphere, there are four saddle point paths passing through each of the four medium directions. Because of symmetry, each has the same real contribution to the action integral  $S_R$ . However, since their azimuths about the easy axis are different, the imaginary part of the action, i.e., the phase  $S_I$ , will not be the same. From the geometrical meaning of the integral in Eq. (3.6), the phase difference between two instanton paths equals  $S$  times the surface area on the unit sphere enclosed by these instanton paths.

To visualize the interference effect we map the two-sphere onto a plane, as in an ordinary atlas (see Fig. 8). The hard axes are mapped onto four equally separated points lying on the equator, and the points exactly halfway between these correspond to the medium axes. Thus, the real projections of the instanton paths can be drawn as curves which start from  $+z$ , pass through the medium points, and end at  $-z$ . The area enclosed by two adjacent instanton paths equals  $\pi$ , since the sphere is equally divided into four paths by the instantons. Thus, the phase difference between adjacent paths becomes  $S\pi$ . Choosing the phase of path 1 as the base, we can perform the summation in Eq. (3.7). Recalling that by symmetry the contribution from real parts of the instanton actions are all same, as are the prefactors  $D_j$ , we have

$$\begin{aligned} \Delta &= D e^{-S_R} e^{-iS_I} (1 + e^{-i\pi S} + e^{-2i\pi S} + e^{-3i\pi S}) \\ &= 4D e^{-S_R} e^{i\gamma} \cos(\pi S) \cos\left(\frac{\pi S}{2}\right), \end{aligned} \quad (3.8)$$

where  $\gamma$  is an irrelevant phase. This result gives us two quenching conditions. From the factor  $\cos \pi S$ , we obtain the quenching of spin tunneling for half-integer  $S$ , which is just the Kramers degeneracy effect. The second cosine implies that the ground state spin tunneling is quenched for odd integer spins, i.e.,  $S = 1, 3, 5$ , etc, and so  $\Delta$  is non-zero only for  $S = 2p$ , where  $p$  is an integer [27].

We now consider the case with  $H_x \neq 0$ . Since the field is assumed to be applied along the  $+x$  axis, both easy and all four medium axes move close to  $+x$  axis. Thus, the two

dimensional picture becomes one as shown in Fig. 9. The four-fold symmetry is now broken, but there are two pairs of instanton paths surrounding the  $+x$  axis:  $(a, a')$  and  $(b, b')$ . The real parts of the instanton actions in a pair are same, but different between the pairs. The phase differences in each pair are the areas enclosed by each pair of instanton paths (the small and large oval regions in Fig. 9) and are dependent on the field  $H_x$ . If we choose the straight line joining  $+z'$  to  $-z'$  as a reference,  $S_{Ia'} = -S_{Ia}$ ,  $S_{Ib'} = -S_{Ib}$ , so that the summation in Eq. (3.7) can be performed as

$$\begin{aligned}\Delta &= D_a e^{-S_{Ra}} \left[ e^{-iS_{Ia}} + e^{-iS_{Ia'}} \right] + D_b e^{-S_{Rb}} \left[ e^{-iS_{Ib}} + e^{-iS_{Ib'}} \right] \\ &= 2D_a e^{-S_{Ra}} \cos \frac{SA_a(H_x)}{2} + 2D_b e^{-S_{Rb}} \cos \frac{SA_b(H_x)}{2},\end{aligned}\quad (3.9)$$

where  $S_{Ra}$ ,  $S_{Rb}$  are the real parts of the instanton actions in each pair, and  $A_a(H_x)$ ,  $A_b(H_x)$  are the areas enclosed by the pairs  $(a, a')$  and  $(b, b')$ , respectively. For  $H_x > 0$  the saddle points through which the paths  $(a, a')$  pass are lower than those for  $(b, b')$ , which means that  $S_{Ra} < S_{Rb}$ . The main contribution to  $\Delta$  in Eq. (3.9) then comes from the first term, and we can neglect the second term. The quenching of the ground state tunnel splitting thus arises when  $A_a(H_x) \simeq (2n + 1)\pi/2S$ , where  $n$  is a non-negative integer. To see how many quenching points are allowed we note that  $A_a(H_x) < A_a(0)$ , where  $A_a(0) = \pi$  (the area enclosed by the two paths 1 and 4 in Fig. 8). From this condition we find  $n < (S - 1)/2$ . For  $S = 10$  there are thus five values of  $H_x$  at which the quenching appears.

The instanton argument provides another way of seeing that the region of very small (but non-zero)  $H_x$  is special. Exactly at  $H_x = 0$ , four instantons are important, but for large  $H_x$  only two are important. There must therefore be a regime of small  $H_x$  where we make a smooth transition between these two behaviors. The width of this regime can be quite small since  $S_{Rb} > S_{Ra}$  as soon as  $H_x \neq 0$ , and these actions appear in the exponents in Eq. (3.9), so that the difference  $(S_{Rb} - S_{Ra})$  is amplified. We thus have another way of seeing why the formula (2.29) fails near  $h_x = 0$ . It contains only cosine factor, and is effectively ignoring the second term in Eq. (3.9).

#### IV. SUMMARY

In this paper, we have used the DPI method to study tunneling in  $\text{Mn}_{12}$ , especially its behavior with a hard-axis field, which is expected to show oscillation as in  $\text{Fe}_8$ . The recursion relation now has nine terms, complicating the analysis. There may be up to five critical curves, which leads to many more turning points. The DPI method still works, however, even though the phase integrals and integrands must be evaluated numerically. But, the numerical procedures required are simple, and involve only root finding and integration in one variable. Except for some special narrow field regions, where two or more turning points merge, the DPI analysis based on linear turning point formulas is extremely good, and agrees with exact numerical results quantitatively.

## REFERENCES

- [1] *Quantum Tunneling of the Magnetization - QTM'94*, edited by L. Gunther and B. Barbara, (Kluwer, Dordrecht,1995).
- [2] W. Wernsdorfer and R. Sessoli, *Science* **284**, 133 (1999).
- [3] A. L. Barra, P. Debrunner, D. Gatteschi, C. E. Schulz, R. Sessoli, *Europhys. Lett.* **35**, 133 (1996);
- [4] C. Sangregorio, T. Ohm, C. Paulsen, R. Sessoli, D. Gatteschi, *Phys. Rev. Lett.* **78**, 4645 (1997).
- [5] T. Ohm, C. Sangregorio, C. Paulsen, *Euro. Phys. J. B* **6**, 195 (1998).
- [6] L. D. Landau and E. M. Lifshitz, *Quantum Mechanics*, 3rd edition (Pergamon, Oxford, U.K., 1976), §90.
- [7] A. Garg, *Europhys. Lett.* **22**, 205 (1993).
- [8] D. Loss, D. P. DiVincenzo, and G. Grinstein, *Phys. Rev. Lett.* **69**, 3232 (1992); J. von Delft and C. L. Henley, *ibid* **69**, 3236 (1992).
- [9] A. Caneschi, D. Gatteschi, and R. Sessoli, *J. Am. Chem. Soc.* **113**, 5873 (1991); R. Sessoli, D. Gatteschi, A. Caneschi, and M. A. Novak, *Nature (London)* **365**, 141 (1993).
- [10] J. Friedman, M. P. Sarachik, J. Tejada, and R. Ziolo, *Phys. Rev. Lett.* **76**, 3830, (1996).
- [11] L. Thomas et al., *Nature* **383**, 145 (1996).
- [12] J. A. A. J. Perenboom, J. S. Brooks, S. Hill, T. Hathaway, and N. S. Dalal, *Phys. Rev. B* **58**, 330 (1998).
- [13] A. L. Barra, D. Gatteschi, and R. Sessoli, *Phys. Rev. B* **56**, 8192 (1997).
- [14] P. A. Braun, *Teor. Mat. Fizika* **37**, 355 (1978) [*Sov. Phys. Theor. Math. Phys.* **37**, 1070 (1978)]; P. A. Braun, *Rev. Mod. Phys.* **65**, 115 (1993).
- [15] J. L. van Hemmen and A. Sütő, *Europhys. Lett.* **1**, 481 (1986); *Physica* **141B**, 37 (1986).
- [16] A. Garg, *J. Math. Phys.* **39**, 5166 (1998).
- [17] A. Garg, *Phys. Rev. Lett.* **83**, 4385 (1999); and submitted to *Phys. Rev. B*.
- [18] A. Garg, math-ph/0003005.
- [19] A. Garg, cond-mat/0003114, cond-mat/0003156.
- [20] J. Villain and A. Fort, *Euro. Phys. J. B.* **17**, 69 (2000).
- [21] G. Herzberg and H. C. Longuet-Higgins, *Discuss. Faraday Soc.* **35**, 77 (1963).
- [22] M. V. Berry and M. Wilkinson, *Proc. Roy. Soc. Lond. A* **392**, 15 (1984).
- [23] This field value, along with some other important ones, is listed in Table I.
- [24] The lower bounds for  $x_1$  and  $x_3$  are found by noting that they arise at  $h_x = 0$ , since for any fixed  $m$ , the curve for  $f(x)$  shifts upward as  $h_x$  is reduced. The lower bound for  $x_2$  (and upper bound for  $x_3$ ) follows from the fact that  $f'(x) = 0$  at  $x = -1/\sqrt{6}$ .
- [25] By writing that  $U_0$  and  $U_{*2,3} = U_i$ , we do not mean that these three critical energies are equal, but that they lie *inside* the classically allowed region.
- [26] M. V. Berry and K. E. Mount, *Rep. Prog. Phys.* **35**, 315 (1972).
- [27] This result also stems from the fourth-order term since it only allows transitions between energy levels with  $\Delta m = 4p$ , where  $p$  is an integer. For spin  $S$  the existence of the ground state tunneling requires  $2S = 4p$ , as before.
- [28] Ersin Keçecioglu and A. Garg, cond-matt/0003319.

FIG. 1. The different types of energy bands possible for recursion relation (2.5) with wavefunction (2.8). Note  $U_\pi(m) = U_+$  in all cases. (a) When  $h_{xr} < h_x < h_{xco}$  with  $|m| < \bar{S}$ , and when  $h_{xc}(m) < h_x < h_{xr}$  with  $|m| > m_*$ . In this case,  $U_0(m) = U_-$ , and  $U_{*1}(m)$  does not appear since  $q_{*1}$  is imaginary. (b) When  $h_{xc}(m) < h_x < h_{xr}$  with  $m_a < |m| < m_*$ . Here,  $U_{*1}(m) = U_-$ ,  $U_0(m) = U_i$ . (c) When  $h_{xi} < h_x < h_{xmax}$  with  $|m| < m_a$ , and when  $0 < h_x < h_{xi}$  with  $m_i < |m| < m_a$ . (d) when  $0 < h_x < h_{xi}$  with  $|m| < m_i$ . Note that, in both (c) and (d),  $U_{*1}(m) = U_-$ , and  $U_0(m)$ ,  $U_{*2}(m)$ , and  $U_{*3}(m)$  are inside the band and thus all denoted  $U_i$ .

FIG. 2. Sketch of the cubic function  $f(x)$  for (a) large  $h_x$ , or large  $|m|$ , (b) small  $h_x$ , or small  $|m|$ . Note that, there is one root in (a), but three roots in (b). The transition from type (a) to type (b) occurs when  $f(-x_m) = f'(-x_m) = 0$  ( $x_m = 1/\sqrt{6}$ ), which gives the curve  $h_{xc}(m)$  in Eq. (2.14).

FIG. 3. The curve  $h_{xc}(m)$  and some physically meaningful values of  $h_x$ 's. In the inset we list these values computed with experimental numbers for  $\lambda_1$  and  $\lambda_2$  for Mn<sub>12</sub>-ac. Points at which  $h_x$  intersects the curve  $h_{xc}(m)$  are  $m = \pm m_a$ .

FIG. 4. The critical curves for Case I. At points  $\pm m_0$ ,  $U_0$  has minima, and the points  $\pm m_c$  denote the intersection between  $E$  and  $U_{*1}$ . Note  $U_{*1} = U_f$  and  $U_0 = U_-$  for all  $|m| \leq \bar{S}$ . For a given value of  $E$ ,  $q$  becomes complex for  $|m| < m_c$  which lies inside the classically forbidden region. In this region the semiclassical wavefunction  $C_m$  oscillates with decaying or growing envelope.

FIG. 5. The critical curves for Case II.  $\pm m_*$  are the points where  $U_0(m) = U_{*1}(m)$  [and  $dU_0(m)/dm = dU_{*1}(m)/dm$ ].  $U_{*1}$  is the lower band edge in the central region  $|m| < m_*$  and forbidden in the outer region  $|m| > m_*$ .

FIG. 6. The critical curves for Case III. (a) When  $h_{xi} < h_x < h_{xmax}$  and (b) when  $0 < h_x < h_{xi}$ . There are five critical curves. Note, however, that  $U_{*2}$  and  $U_{*3}$  appear only in the region  $|m| < m_a$  because they are complex outside this region.

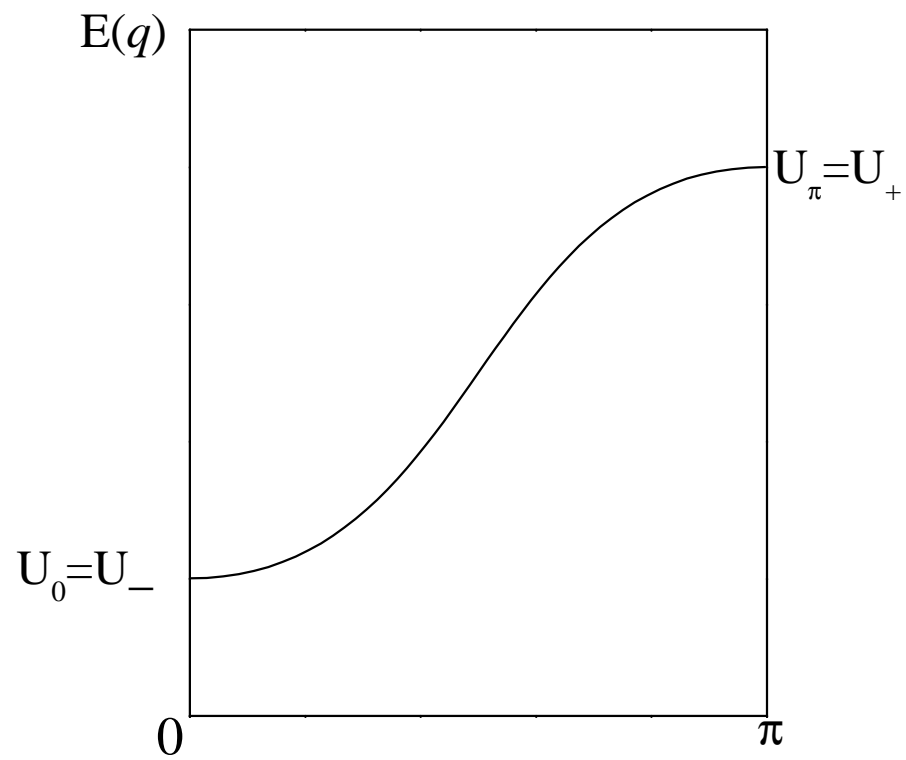
FIG. 7. Tunnel splittings  $\Delta_n$  between first three pairs of levels as a function of the field parameter  $h_x$ . The dotted and solid curves are obtained from exact numerical diagonalization of the Hamiltonian and the DPI method, respectively.

FIG. 8. Two dimensional picture of instanton paths when  $H_x = 0$ . The points  $\pm x$ ,  $\pm y$  are the hard axes, and  $m_i$ 's represent the medium axes. Dotted lines denote the real projections of the instanton paths.

FIG. 9. Two dimensional picture of instanton paths when  $H_x \neq 0$ . The points  $\pm z'$  represent the new easy axes. The instanton paths are again denoted by dotted lines. Note that the areas enclosed by each pair of instanton paths are shrunk due to the field.

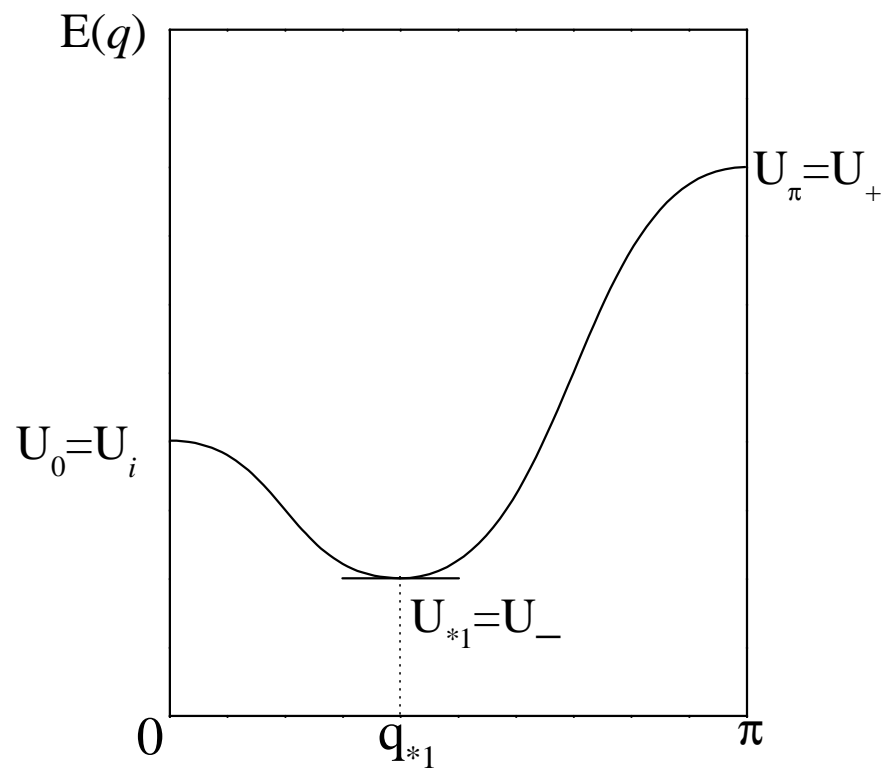
TABLE I. Physical meanings of the special  $h_x$ 's

$h_{xco}$	Coercive field above which no tunneling exists.
$h_{xosc}$	The value below which the wavefunction can have an oscillating part inside the forbidden region.
$h_{xr}$	The value above which $q_{*1}$ becomes real.
$h_{xmax}$	The maximum value of the curve $h_{xc}(m)$ .
$h_{xi}$	The value at which $U_{*3}(0)$ intersects $U_0(0)$ .



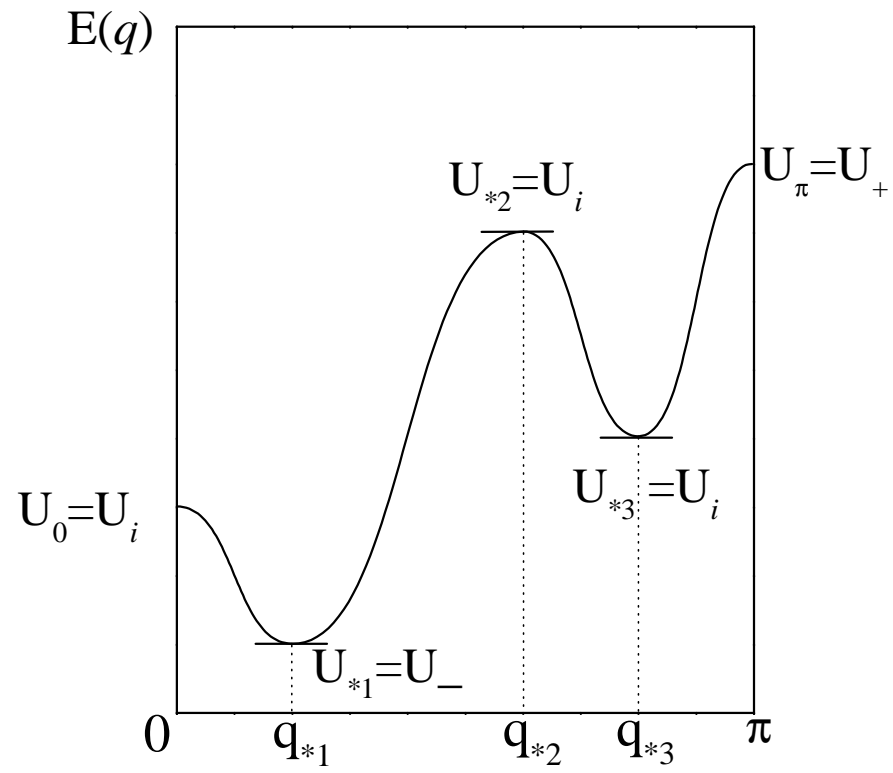
(a)

Fig.1a



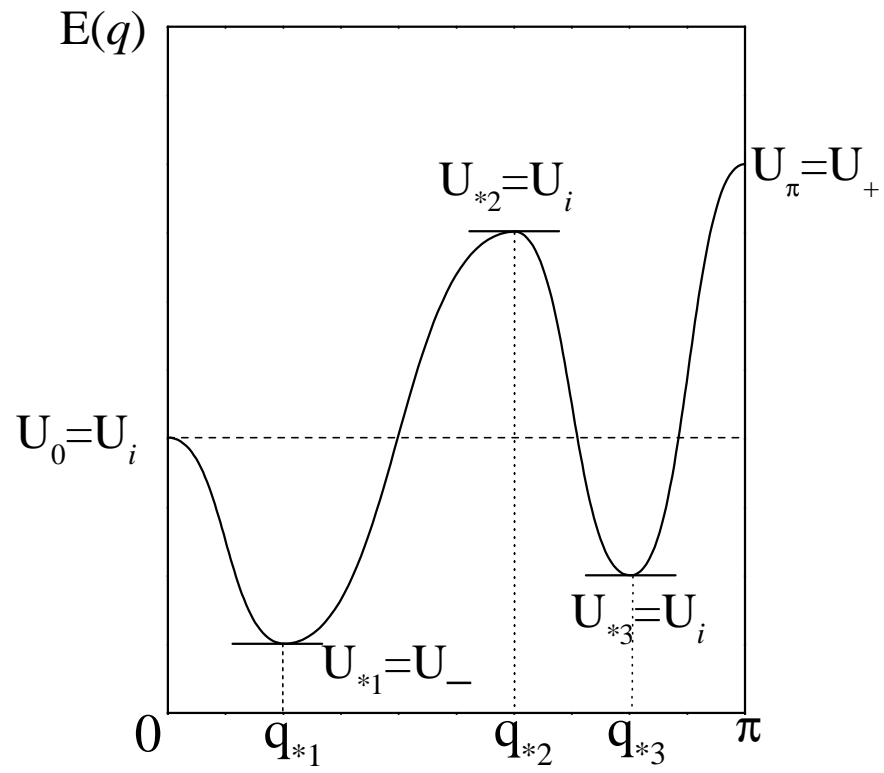
(b)

Fig.1b



(c)

Fig.1c



(d)

Fig.1d

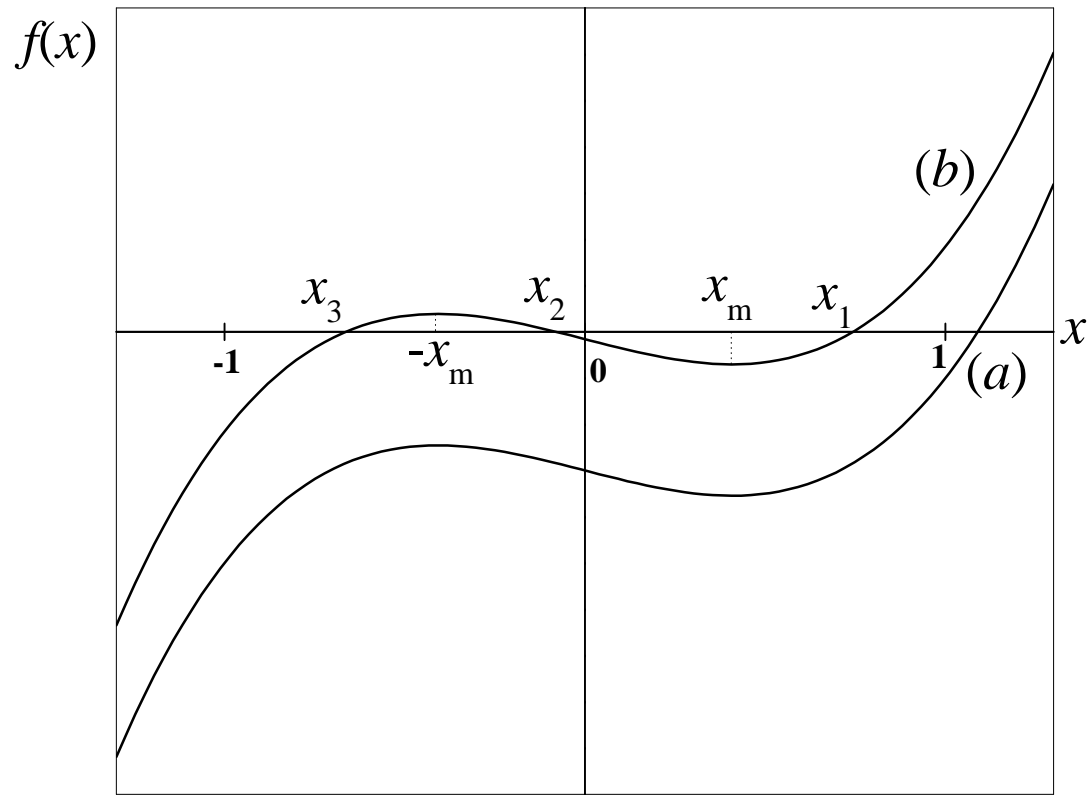


Fig.2

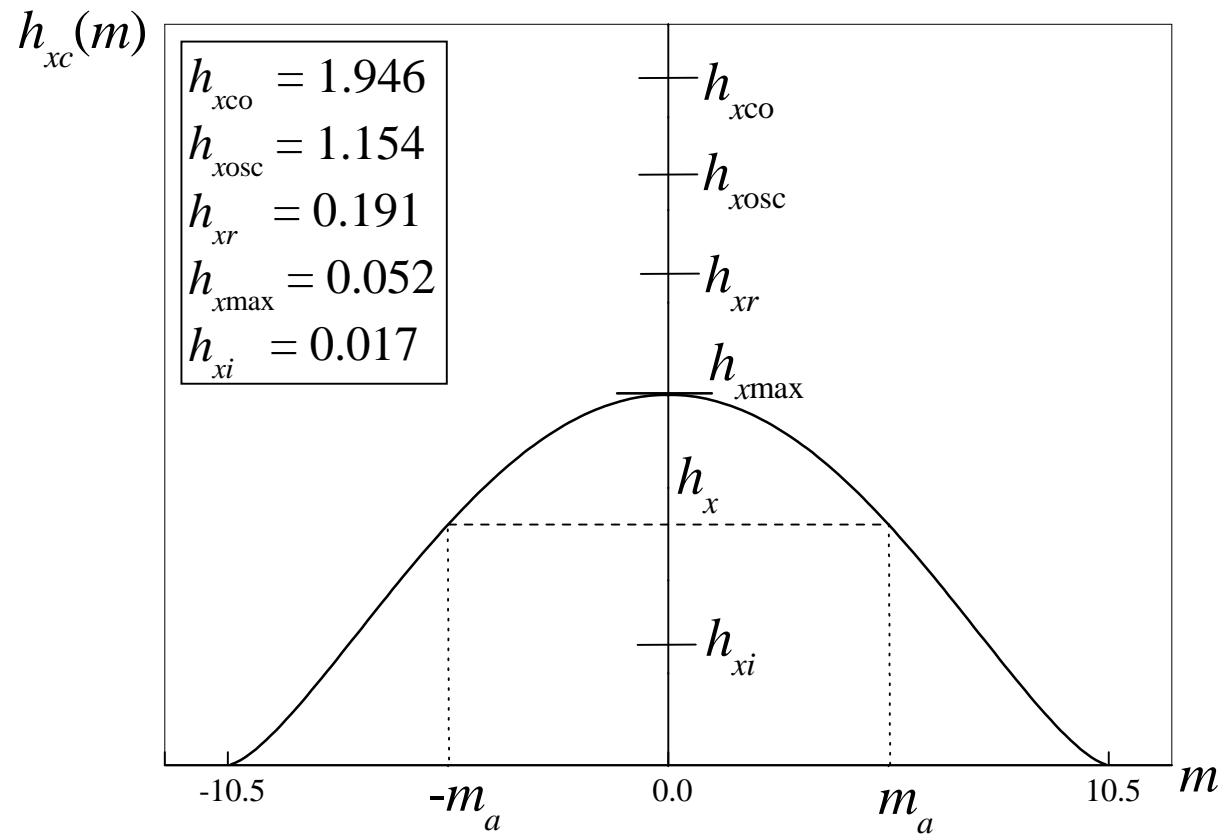


Fig.3

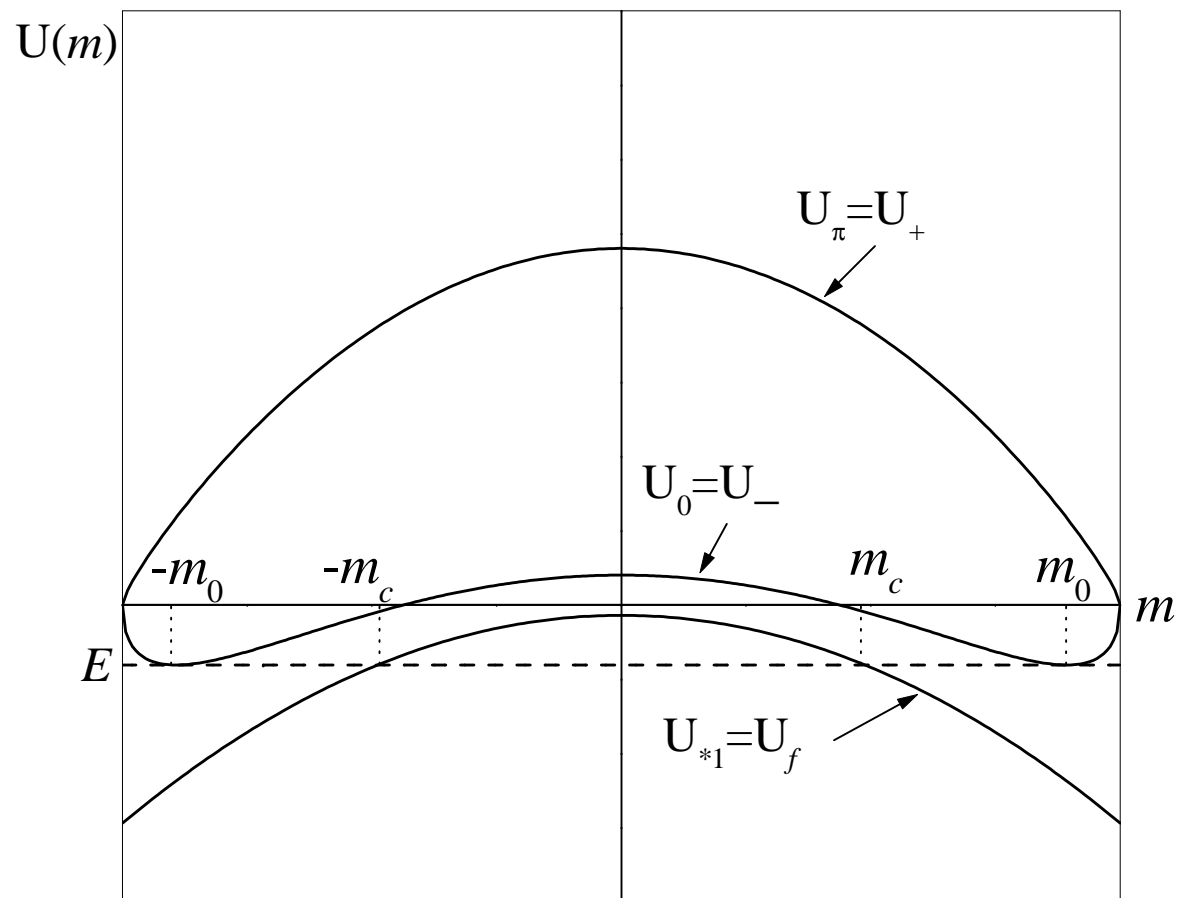


Fig.4

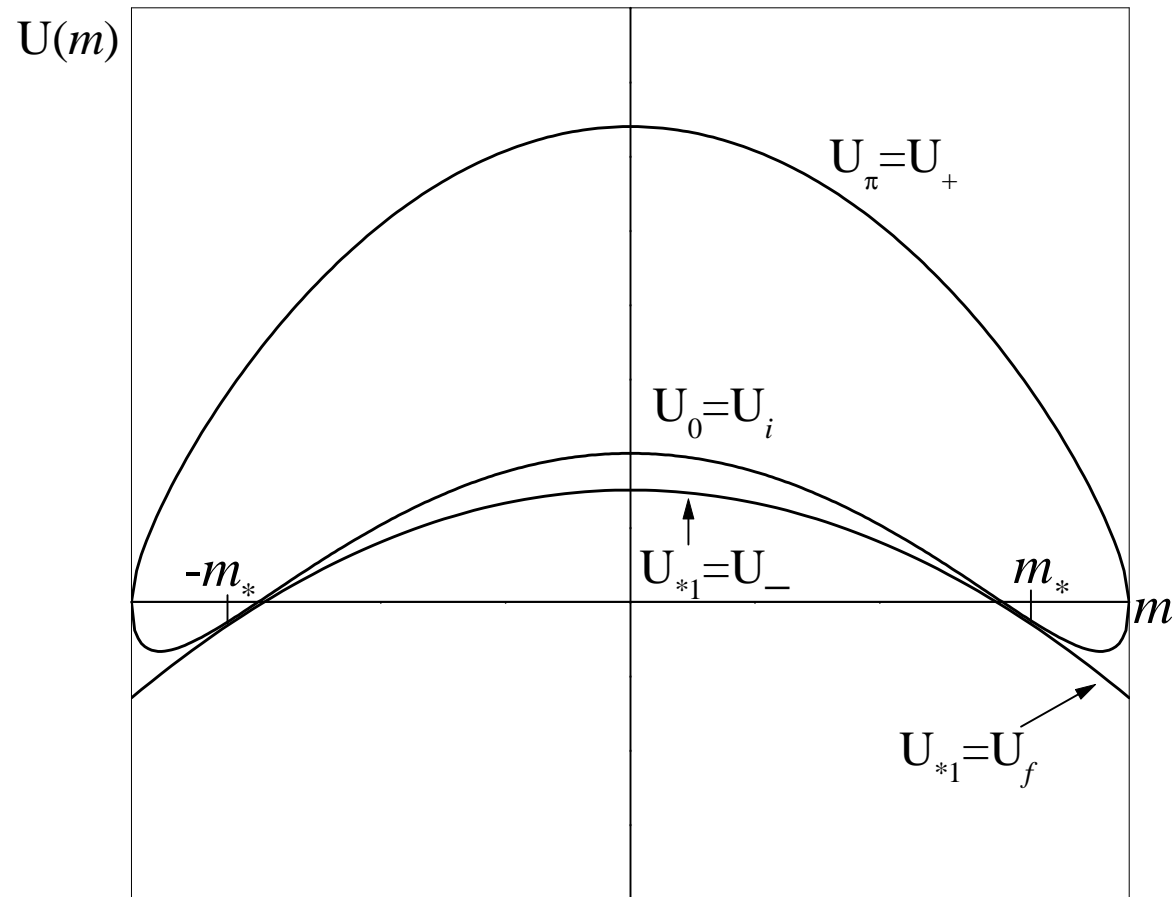
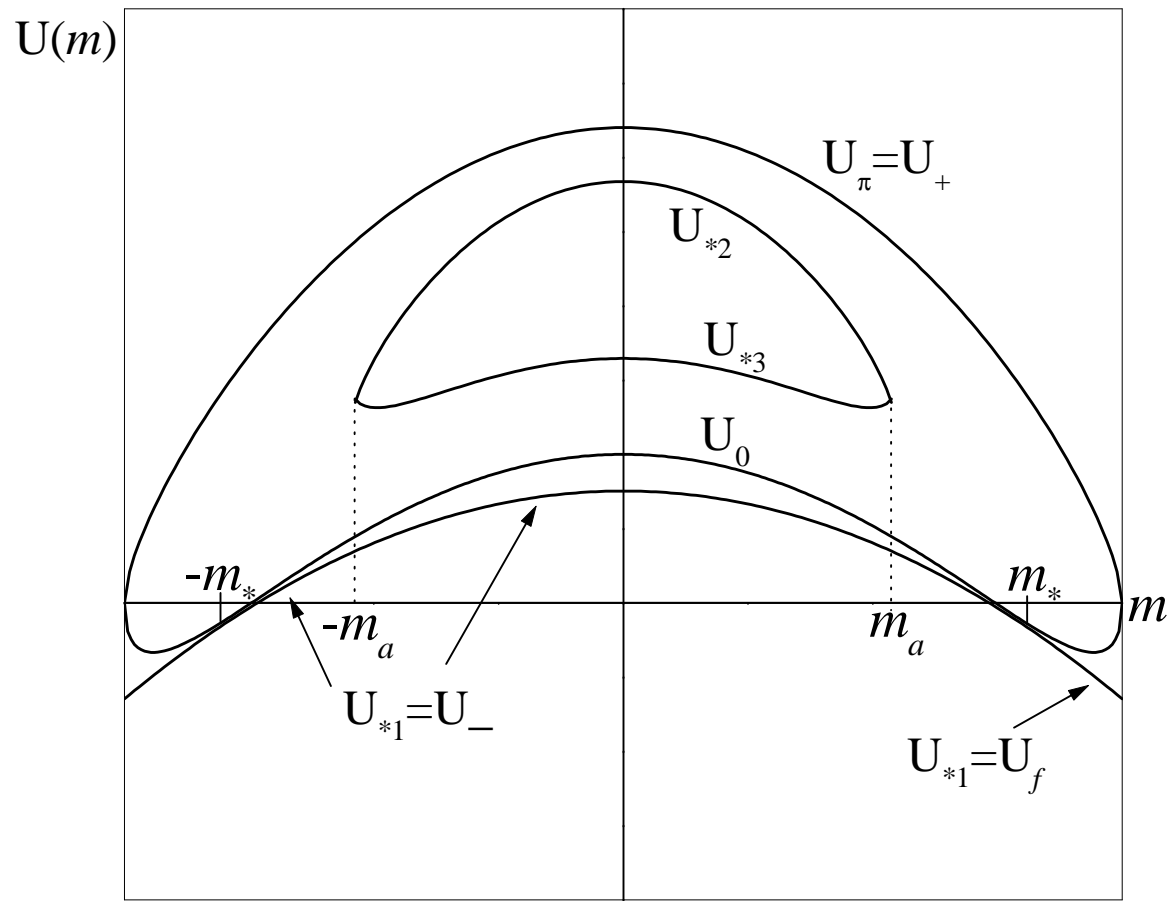
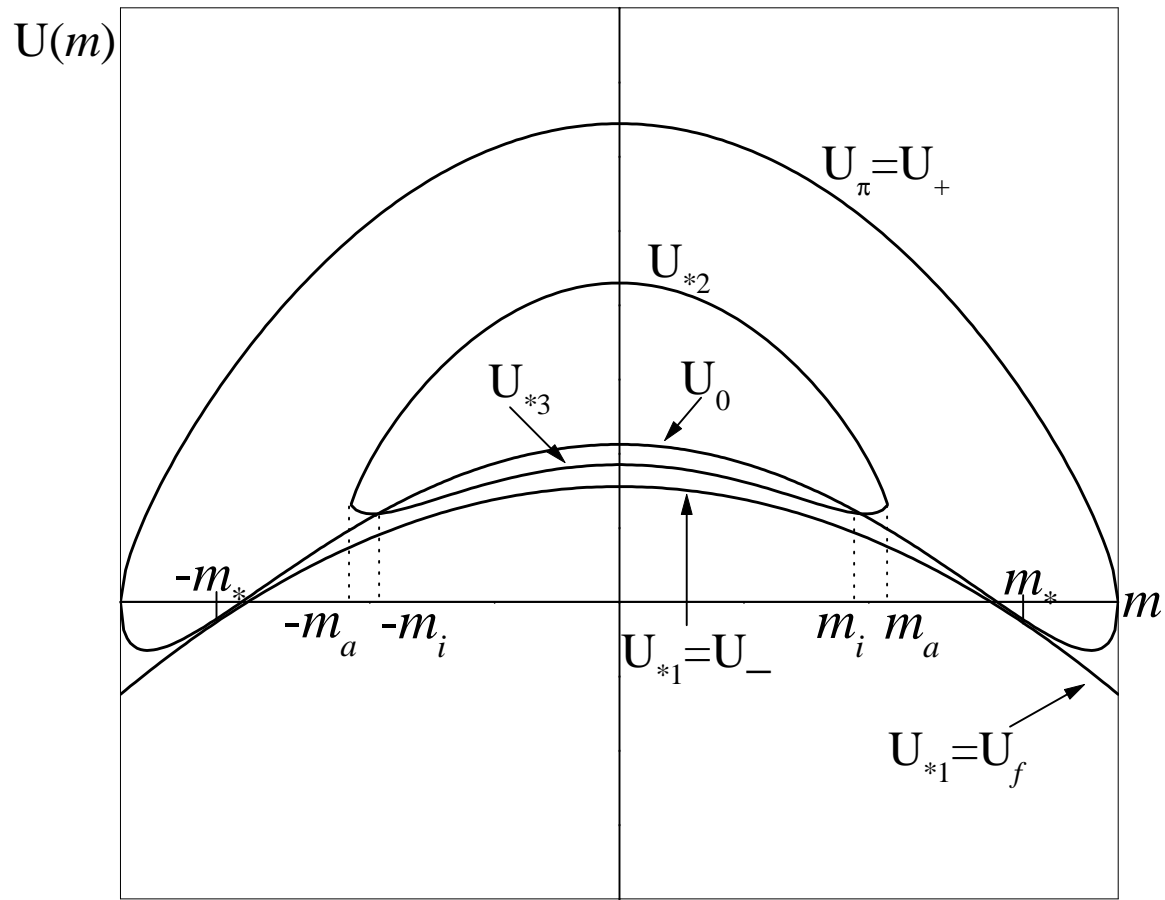


Fig.5



(a)

Fig.6a



(b)

Fig.6b

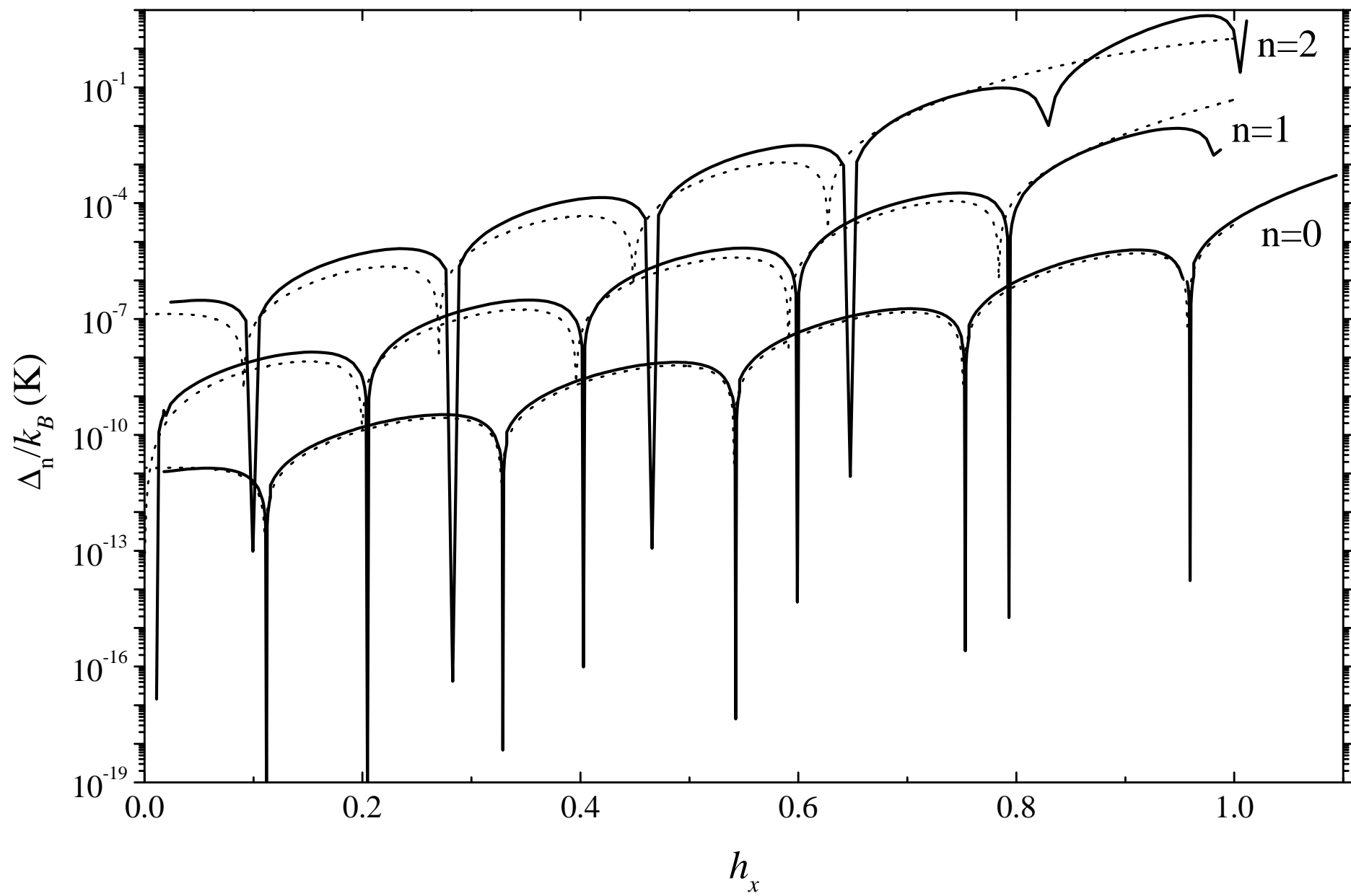


Fig.7

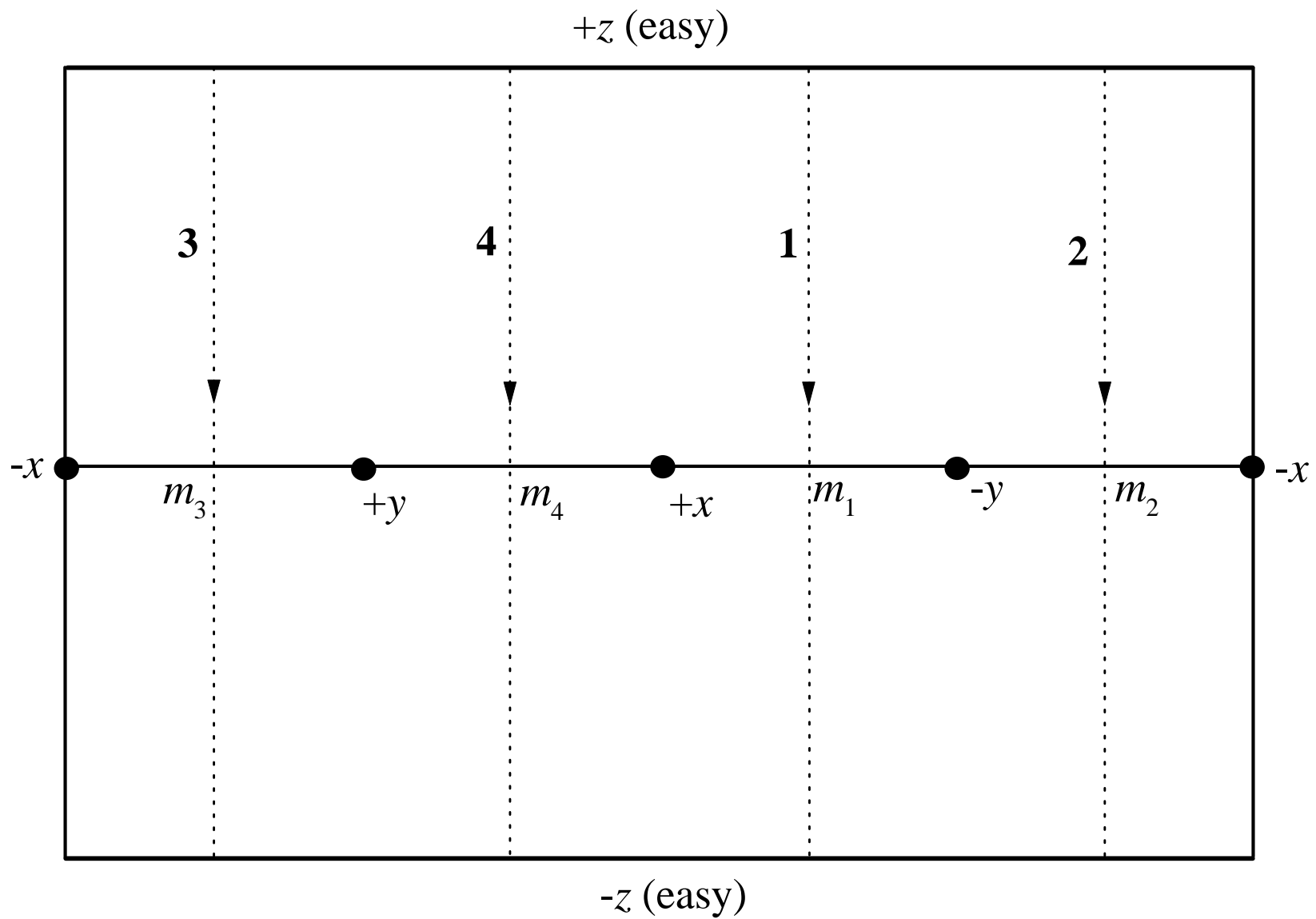


Fig.8

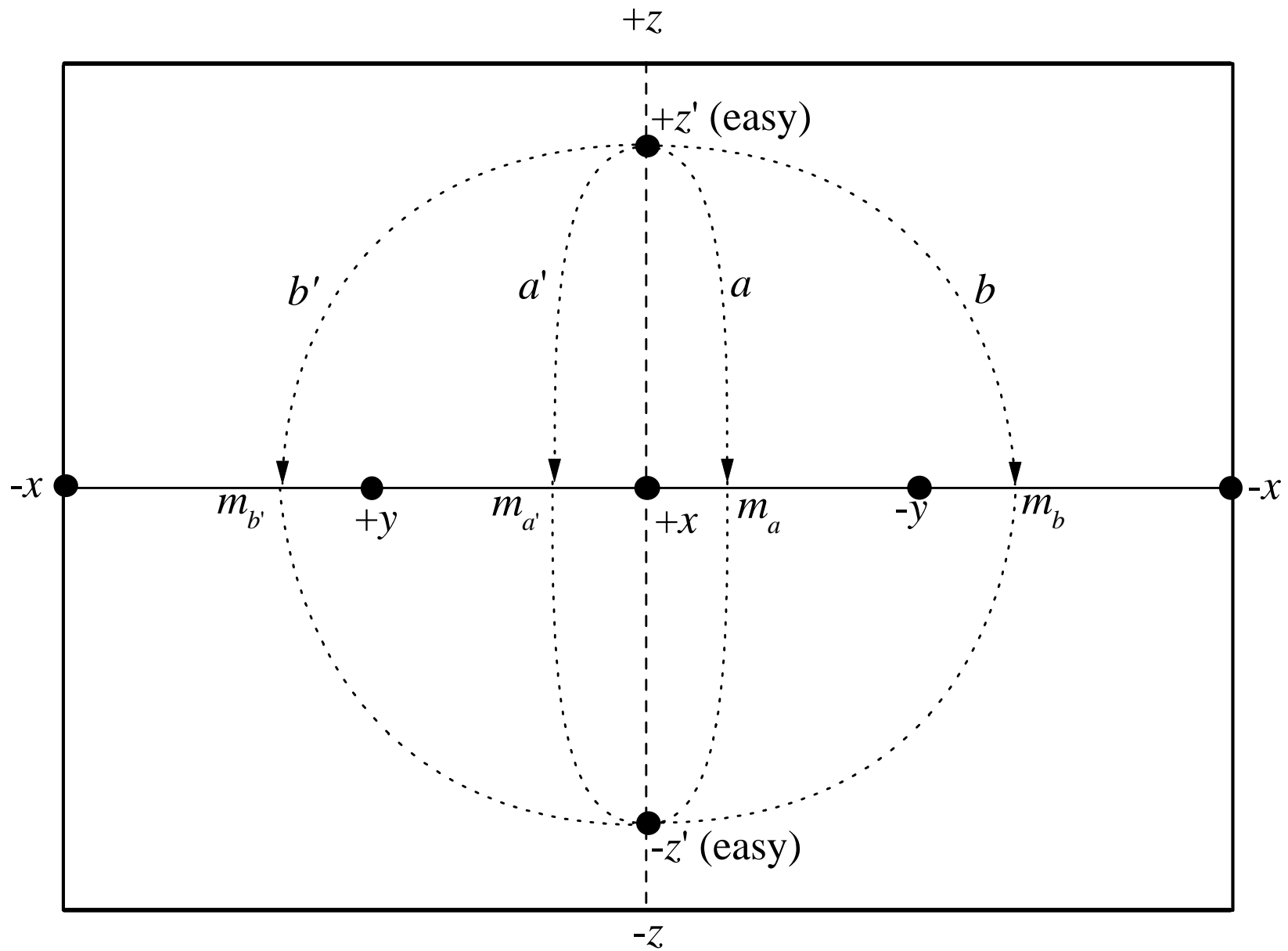


Fig.9